Mechanics and Mechanical Engineering
Vol. 17, No. 2 (2013) 207–220


# Sensitivity to Imperfections of Perforated Pallet Rack Sections

Viorel Ungureanu
Dan Dubina
*Department of Steel Structures and Structural Mechanics*
*Civil Engineering Faculty*
*"Politehnica" University of Timisoara*
*Ioan Curea 1, 300224 Timisoara, Romania*
*Laboratory of Steel Structures*
*Romanian Academy – Timisoara Branch*
*Mihai Viteazu 24, 300223 Timisoara, Romania*

Received (11 March 2013)
Revised (16 April 2013)
Accepted (20 May 2013)

The paper analyses the influence of imperfections on the behaviour of perforated pallet rack members in compression using non-linear FE simulations. The effect of imperfections, perforations and buckling modes, reduces significantly the capacity of perforated members in compression, especially in the coupling range due to interaction. A sensitivity analysis done using calibrated and validated numerical models can be done in order to determine the most detrimental combinations of imperfections to be considered for numerical simulations. The ECBL approach can be successfully applied to perform a sensitivity analysis via numerical simulations, using a limited number of experimental tests.

*Keywords*: Cold formed section, sensitivity analysis, ECBL method.

## 1. Introduction

All structures are in reality imperfect. The imperfections refer to cross–section and member geometry, to residual stresses and to yield strength distribution across the section, to supporting conditions of the members and to load introduction. Excepting the last two types of imperfections, which are of mechanical type, a lot of work has been done to analyse, classify and codify the material and geometrical imperfections [1–6].

It was observed the different nature of imperfections, associated with the slenderness of component walls, leads to different instability behaviour of cold–formed sections compared to hot–rolled ones [1]. As a consequence, specific buckling curves should be provided for cold–formed steel sections instead of using European buckling curves obtained for hot–rolled ones.

Due to the local and distortional instability phenomena, and their coupling with overall buckling modes, the post-critical behaviour of thin-walled cold-formed steel members is highly non-linear, being very difficult to be predicted using analytical methods. Numerical non–linear analysis can be successfully used to simulate the real behaviour of cold–formed steel sections. Initial imperfections as equivalent sine shapes, with half-wave lengths corresponding to relevant buckling modes are used as geometric non–linearity. Rasmussen & Hancock [7] and Schafer & Peköz [2] proposed numerical models, to generate automatically geometrical imperfection modes into the non–linear analysis. To define the relevant sine imperfection modes, Schafer et al. [8] used the probabilistic analysis in order to evaluate the frequency and magnitude of imperfections.

Related to numerical models and methods applied in the simulation, two general reports, presented in two editions of *Coupled Instability in Metal Structures* conferences, CIMS 1996 and CIMS 2000, by Rasmussen [9] and Sridharan [10], reviewed the main contributions and milestones in the progress at the date. They concluded the most used computational models are the ones applying the semi–analytical and spline finite strip and the finite element methods. At CIMS 2008, summarizing the advances and developments of computational modelling of cold-formed steel elements, Schafer [11] emphasized that the primarily focus is the use of semi–analytical finite strip method, considering the implementation of the constrained finite strip method (cFSM) [12]. This method allows for discrete separation of local, distortional and global deformations, and collapse modelling using shell finite elements.

A good alternative to that is the application of modal decomposition via Generalised Beam Theory (GBT), method which achieved a significant development in the last decade by works of the Lisbon team led by Camotim [13], which makes possible to select the deformation modes to be considered in the analysis.

Camotim et al. [14] summarise the main concepts and procedures involved in performing a GBT buckling analysis together with the development and numerical implementation of a GBT–based beam finite element formulation, which includes local, distortional and global deformation modes and can handle general loadings. Camotim and Dinis [15] have performed extended numerical studies, using FEM and GBT, to study the elastic post-buckling behaviour of cold–formed steel columns affected by mode interaction phenomena involving distortional buckling, namely local/distortional, distortional/overall (flexural–torsional) and local/distortional/overall mode interaction and also sensitivity to imperfections of thin–walled cold–formed steel members.

Loughlan et al. [16] analysed the behaviour of lipped channel profiles in compression considering the local–distortional interaction, including material yielding and yield propagation to ultimate conditions and then to elastic-plastic unloading. The effects of geometric imperfections were also considered in the numerical simulations.

Based on numerical simulations Dubina & Ungureanu [5,6] have systematically studied the influence of size and shape of sectional geometrical imperfections and the erosion of theoretical buckling strength on the behaviour of cold–formed steel plain and lipped channel sections., both in compression and bending.

However, despite this numerical progress and, even if there is an important

number of existing investigations devoted to the effect of holes on cold–formed steel members, there is not yet an analytical design procedure for pallet rack columns to be accepted by the professional community. In what concerns the possibility to apply numerical methods used, at this moment GBT and FSM cannot model members with perforated walls, except if using an equivalent thickness; in such circumstances FEM remains the only approach available to model perforated walls, but with the price of a costly work.

Casafont et al. [17] present an investigation on the use of the Finite Strip Method to calculate elastic buckling loads of perforated cold–formed storage rack columns. Due to the fact that holes cannot be directly modelled with FSM, the concept of the reduced thickness of the perforated strip was applied to take into account their effect. A formulation was presented for the reduced thickness that has been calibrated with loads obtained in eigen buckling FEM analyses. Bonada et al. [18] presented three numerical methodologies to predict the compression load carrying capacity of cold–formed steel rack section without perforations. The three methodologies allow for different imperfection shapes. The first one uses the critical mode shape (the first buckling mode). The second corresponds to an iterative methodology in which the shape that leads to the lowest ultimate load is used. These two first methodologies use exclusively the finite element method (FEM). The third one combines the finite element analysis with the generalised beam theory (GBT) in order to determine the modal participation of the FEM buckling mode and generate a particular combined geometric imperfection.

Besides stability problems, the material changes due to cold–forming influences the ultimate capacity of pallet rack upright sections. Armani et al. [19] investigated, by numerical simulations, the effects of local changes of the material properties due to the strain-hardening associated with cold–forming and the role of the initial geometrical imperfections when the uprights are subject to axial load.

Present paper presents the numerical approach for the study of buckling modes interaction (distortional and overall) for pallet rack members in compression. A numerical imperfection sensitivity study was conducted in order to determine the maximum erosion of critical bifurcation load due to mode coupling, imperfections and perforations. Using the ECBL approach [20] the maximum value of erosion was computed and based on its value, a corresponding $\alpha$ imperfection factor, in order to adapt the actual European buckling curves for cold–formed pallet rack sections.

## 2. Experimental program

An intensive experimental study on pallet rack uprights in compression has been carried out at the "Politehnica" University of Timisoara. The experimental program was extensively presented by the authors in [21, 22].

Both perforated and unperforated section specimens have been tested, of calibrated lengths for: stub columns (s) [24]; upright member specimens for distortional buckling (u) [24]; specimens of lengths equal with the half–wave length for distortional buckling (d); specimens of lengths corresponding to interactive buckling range (c). Two cross–sections of the same typology but different sizes, RS125×3.2 and RS95×2.6, have been considered, of perforated–to–brut cross–section ratios ($A_N/A_B$) of 0.806 and 0.760, respectively.

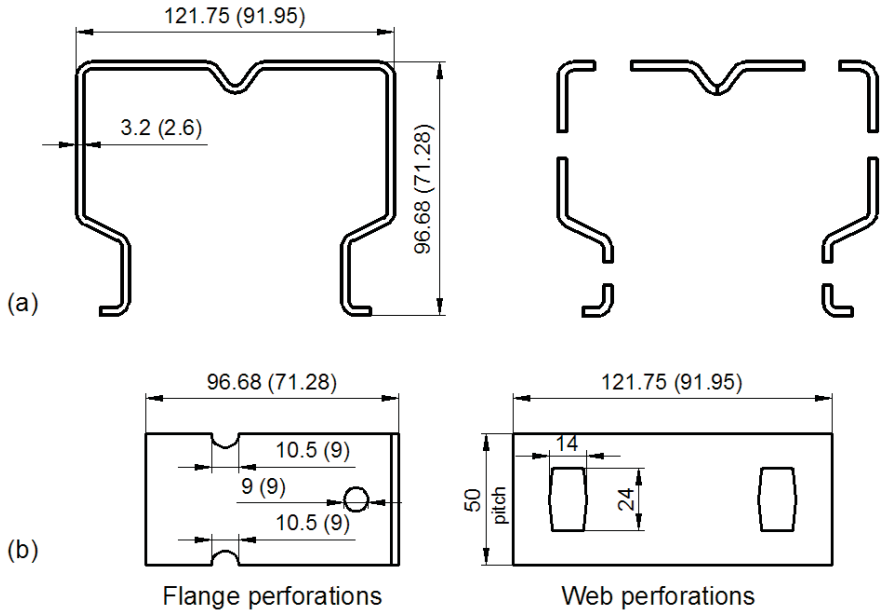


**Figure 1** (a) Brut and perforated specimen cross-section; (b) perforation details

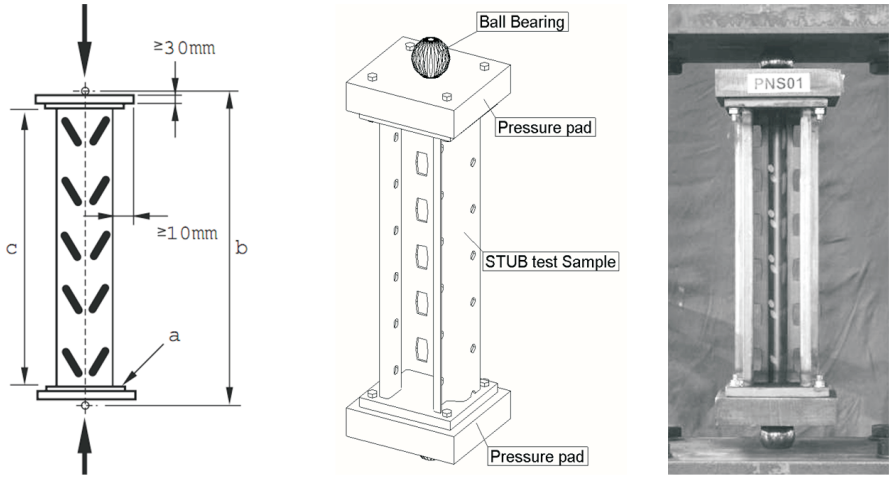


**Figure 2** Stub column test setup

Their brut and perforated (i.e. net) sections are shown in Fig. 1 together with the perforations details. The pitch is 50mm for both studied sections. The test setup was the same for all tested specimens. The test setup for stub column test is presented in detail in Fig. 2. The ball bearing was positioned on the symmetry axis of the cross–section in between the position of gross and the minimum cross–section centres of gravity. Additional restraints were foreseen for specimens of lengths corresponding to interactive buckling range (c) in order to restrain the torsion.

Tab. 1 presents the failure modes for each type of the tested specimen/section. The following notations were used: S – Squash, DS – symmetrical distortional buckling, FT – flexural-torsional buckling, F – flexural buckling.

**Table 1** Failure modes for tested sections

| Section<br>Test type | RS95×2.6<br>brut | RS95×2.6<br>perforated | RS125×3.2<br>brut | RS125×3.2<br>perforated |
|---|---|---|---|---|
| Stub (s) | S | S/DS | DS | DS |
| Distortional (d) | DS | DS | DS | DS |
| Upright (u) | F or FT | F or FT | DS | DS |
| Interactive buckling (c) | DS+F or DS+FT | DS+F or DS+FT | DS+F or DS+FT | DS+F or DS+FT |

Additional experimental tests have been done in order to determine the mechanical properties of the material. A set of samples were tested from the base material. Due to cold-forming process of the cross–section, the material properties are modified. New series of tests on coupons cut over the cross-section of specimens without perforations was done for both types of sections, in order to determine the increase of yield strength, ultimate tensile strength and residual stresses [21, 22]. Fig. 3 shows, as an example, the measured values of yield strength and residual stresses distributions for RS125×3.2 brut cross–section, as percent of yield strength of base material.

In what concerns the geometric imperfections, all tested specimens were measured. Two types of imperfections were recorded, i.e. (a) sectional and (b) global [21,22]. The sectional geometric imperfections range for RS125×3.2 cross–section, between –3.10 mm ... +1.64 mm, while for RS95×2.6 cross–section between –2.93 mm ... +2.74 mm. Similar values for this type of imperfection were mentioned by Schafer & Peköz [2] in their studies. The global imperfections, represented by the mid span deflections, on both $y$ and $z$ direction, were obtained matching the measured deflection with a half-wave sine equivalent (see Fig. 6). The maximum recorded values of global imperfections in $z$ direction were $L/1416$ for RS95×2.6 cross–section and $L/1651$ for RS125×3.2 one, while in $y$ direction the maximum values were found to be less than $L/3500$ for both sections, with and without perforations. The measured global imperfection (overall sinusoidal imperfections) are significantly lower than the less conservative value, of $L/1000$, proposed by ECCS Recommendation [25] and considered for European buckling curves. On the other hand, the corresponding tolerance accepted by EN1090–2 [26] is $L/750$.

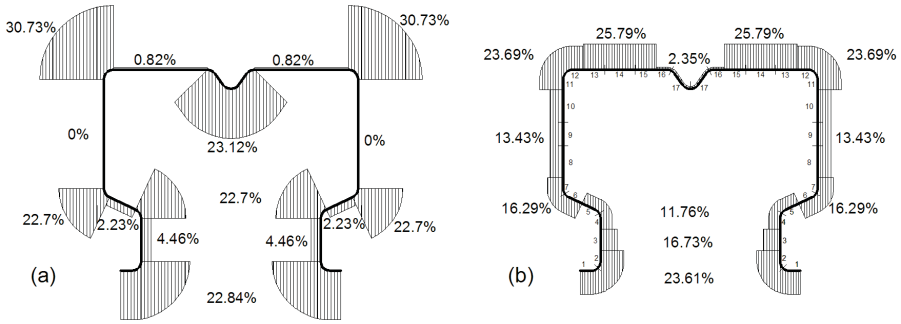


**Figure 3** (a) Yield strength distribution ($\%f_y$); (b) Residual stress distribution ($\%f_y$) represented on the compressed side of the strip (RS125 brut cross–section)

## 3. Numerical model calibration and validation

Numerical models applied to simulate the behaviour of studied sections, have been created using the commercial FE program ABAQUS/CAE. The numerical models were calibrated to replicate the physical experimental tests. Rectangular 4–noded shell elements with reduced integration (S4R) were used to model the thin–walled cold–formed members. In order to create a reliable mesh and to account the holes present along the specimen's length a mesh size of about 5×5 mm was chosen. In the calibration process it was found that the influence of residual stress is small (less than 3%) and their effects will be ignored further in the analysis [21, 23].

The base plates and pressure pads were modelled using RIGID BODY with PINNED nodes constraints. The reference point for the constraints was considered the centre of the ball bearings (55 mm outside the profile), in the gravity centre of the cross–section. For numerical simulations, the specimens were considered pinned at one end and simply supported at the other one. For the pinned end, all three translations together with the rotation along the longitudinal axis of the profile were restrained, while the rotations about maximum and minimum inertia axes were free. For the simply supported end, the translations along section axis and the rotation about longitudinal profiles axis were restrained, while the rotations about major and minor inertia axis together with longitudinal translation were allowed. For the tested specimens the rotation about longitudinal axis was prevented by friction, while in numerical model the rotation was restrained, to remove rigid body displacements.

The analysis was conducted into two steps. The first step consists into an eigen buckling analysis (LBA), in order to find a buckling mode or combination of buckling modes, affine with the relevant measured imperfections. After, imposing the initial geometric imperfection, obtained as a linear combination of eigen buckling modes from the previous step, a GMNIA analysis with arc–length (static, Riks) solver was used to determine the ultimate capacity of pallet rack members in compression. A unit displacement was applied at the simply supported end, incremented during the analysis, in order to simulate a displacement controlled experimental test.

It must be underlined that for all considered numerical models, the failure

modes were in accordance with the failure modes observed in experimental tests (see Fig. 4). The calibrated numerical model was validated against experimental tests for all tested sets of profiles. Tab. 2 presents the values of ultimate load from numerical simulations and the experimental ones for all types of members ((s), (u), (d), (c)), for both RS125×3.2 and RS95×2.6 cross–sections, with and without perforations.

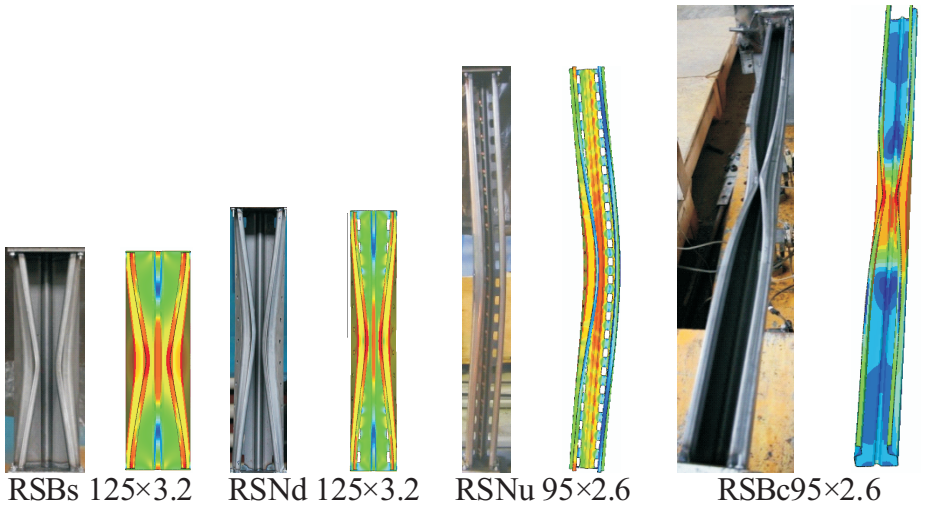


**Figure 4** Failure modes – Experimental vs. FE models

Based on the results obtained from numerical simulations, it can be noted that from the point of view of maximum load, the numerical model is able to accurately replicate the experimental tests. For specimens with increased length, where global and sectional imperfections are of same importance, a more complex imperfections measurement is recommended. The measurements should allow the decomposition of geometric imperfections into sectional and global components that can afterwards be used to reconstruct the initial deformed shape.

## 4. Imperfection sensitivity analysis

### 4.1. *Determination of coupling point using ECBL approach*

The interactive buckling approach based on ECBL method was largely presented in [20]. The principle of this method is summarized here only. Assuming the two theoretical simple instability modes that couple, in a thin-walled compression member, are the Euler bar instability mode, $\overline{N}_E = 1/\overline{\lambda}^2$ ($\overline{\lambda}$ = relative member slenderness) and the distortional instability mode described by means of the reducing factor of area $\overline{N}_D$. The resulting eroded curve for coupled instability mode is $\overline{N}(\overline{\lambda}, \overline{N}_D, \psi)$ (see Fig. 5).

**Table 2** Ultimate load [kN] – Experimental vs. FEM

| RSBs125×3.2 | | RSNs125×3.2 | | RSBs95×2.6 | | RSNs95×2.6 | |
|---|---|---|---|---|---|---|---|
| EXP | FEM | EXP | FEM | EXP | FEM | EXP | FEM |
| 487.05 | 486.13 | 411.02 | 422.98 | 338.88 | 335.15 | 274.33 | 272.01 |
| RSBd125×3.2 | | RSNd125×3.2 | | RSBd95×2.6 | | RSNd95×2.6 | |
| EXP | FEM | EXP | FEM | EXP | FEM | EXP | FEM |
| 440.79 | 440.78 | 394.62 | 397.04 | 325.10 | 331.05 | 262.67 | 255.47 |
| RSBu125×3.2 | | RSNu125×3.2 | | RSBu95×2.6 | | RSNu95×2.6 | |
| EXP | FEM | EXP | FEM | EXP | FEM | EXP | FEM |
| 386.72 | 384.40 | 347.26 | 344.00 | 279.65 | 285.96 | 223.33 | 231.89 |
| RSBc125×3.2 | | RSBc125×3.2 | | RSBc95×2.6 | | RSBc95×2.6 | |
| EXP | FEM | EXP | FEM | EXP | FEM | EXP | FEM |
| 317.89 | 316.67 | 293.62 | 292.9 | 220.29 | 220.26 | 168.88 | 177.11 |

(s) Stub columns;
(d) Specimens of lengths equal with the half–wave length of distortional buckling;
(u) Upright member specimens;
(c) Specimens of lengths corresponding to interactive buckling range;
N/B – perforated/brut

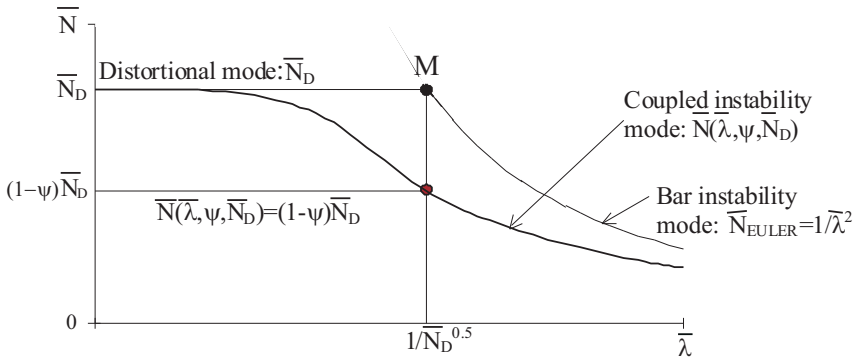


**Figure 5** The interactive buckling model based on the ECBL theory

The maximum erosion of critical load, due both to the imperfections and coupling effect, occurs in the interaction point, M ($\overline{\lambda} = \sqrt{1/\overline{N}_D}$) where, the erosion coefficient $\psi$ is defined as:

$$\psi = \overline{N}_D - \overline{N} \tag{1}$$

in which $\overline{N}(\overline{\lambda}, \overline{N}_D, \psi)$ is the relative interactive buckling load and $\overline{N}_D = N_D/f_yA$; $A$ = is the cross–section area; $N_D$ = is the ultimate capacity corresponding to distortional buckling; $\overline{N} = N/f_yA$ is the relative axial load; $N$ = is the axial load.

If $\overline{\lambda} = \sqrt{1/\overline{N}_D}$ is introduced, it results an imperfection factor corresponding to distortional–global buckling:

$$\alpha = \frac{\psi^2}{1-\psi} \cdot \frac{\sqrt{\overline{N}_D}}{1 - 0.2\sqrt{\overline{N}_D}} \tag{2}$$

Eqn. (2) represents the new formula of $\alpha$ imperfection factor which should be introduced in European buckling curves in order to adapt these curves to distortional-overall interactive buckling.

The coupling point between distortional (D) and global (F) buckling modes is determined following the ECBL approach as shown in Fig. 4. On this purpose, FE analyses were performed to simulate the influence of different types of imperfections in the coupling point. Because the interest is to observe the erosion of critical bifurcation load, the ECBL approach is applied considering the distortional critical load, obtained for the relevant section by an eigen buckling analysis (Linear Buckling Analysis (LBA) using ABAQUS), in interaction with Euler buckling of the corresponding bar member. Tab. 3 shows the reference values for critical and ultimate sectional loads obtained numerically and experimentally for the studied sections.

**Table 3** Sectional capacity and distortional buckling load

| Section | RSN125×3.2 | RSN95×2.6 |
|---|---|---|
| Length [mm] | 600 | 500 |
| Distortional buckling load* ($N_{cr,D}$) [kN] | 370.48 | 340.78 |
| Distortional ultimate load** ($N_{D,u}$) [kN] | 388.35 | — |
| Stub ultimate load*** ($N_{S,u}$) [kN] | 407.79 | 279.27 |
| Squash load**** ($N_{pl}$) [kN] | 480.94 | 286.72 |
| * distortional buckling load determined using LBA;<br>** experimental failure load corresponding to "distortional" specimens – mean values;<br>*** experimental failure load corresponding cu stub column specimens – mean values;<br>**** $N_{pl} = A \cdot f_y$ | | |

Tab. 4 presents the lengths corresponding to the theoretical interactive buckling loads (e.g. in the point of $\overline{\lambda} = \sqrt{1/\overline{N}_D}$, $\overline{N}_D = \overline{N}_{cr,D}$) determined via the ECBL approach, in the interactive buckling point, M, for each section.

It can be observed that for RS95N cross–sections, the critical load corresponding to distortional buckling is greater than the cross-section squash load. In this case the $\overline{N}_D$ value has to be limited to 1.00. Based on this limitation, for RS95 section,

**Table 4** Lengths corresponding to the theoretical interactive buckling

| Profile | $N_{cr,D}$ [kN] | $N_{pl}$ [kN] | $\overline{N}_D$ | Coupling length [mm] |
|---|---|---|---|---|
| RSN125 | 370.48 | 480.94 | 0.770 | 2559 |
| RSN95 | 340.78 | 286.72 | 1.000 | 1667 |

with and without perforation, there is no classical interactive buckling, but we could speak about a local plastic – elastic buckling interaction.

### 4.2. *Imperfection sensitivity study*

On the following, the study focuses on the sensitivity to imperfections of pallet rack sections in compression, having the member length equal to the interactive buckling length, established according to ECBL approach, presented in the previous subchapter.

An imperfection sensitivity analysis was conducted in order to identify the most critical imperfection or combination of imperfections. Fig. 6 shows the types of geometrical imperfections considered in the analysis, i.e. distortional (d ±), flexural about the minor axis (f ±), and coupling of these two (f ± d ±). Also, load eccentricities, located on the axis of symmetry, were taken into consideration, with different amplitudes. In case of flexural–torsional buckling (FT), both initial deflection and initial twisting imperfection (ft) were considered together, according to Australian Standard AS4100 [23,27].

Detailing, the imperfections used for this study are: distortional symmetric imperfection (ds), distortional asymmetric imperfection (da) (only for RSN125×3.2 section), flexural bow imperfection about the minor inertia axis (f), loading eccentricities on both axes (independent and coupled, i.e. EY, EZ, EY–EZ) and flexural-torsional imperfection (ft). The distortional imperfection, symmetric and asymmetric, was scaled to $0.5t$, $1.0t$ and $1.5t$, the flexural bow imperfection was scaled to $L/750$, $L/1000$ and $L/1500$, while the flexural-torsional imperfection was considered in accordance with the provisions of Australian Standard [27]. The loading eccentricities were varied on both sectional axes (±2mm; ±4mm; ±6mm), independently and together, as an oblique eccentricity.

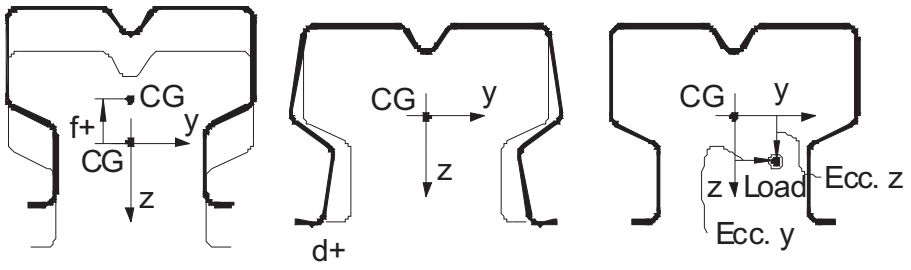


**Figure 6** Example of considered simple imperfections (f and d)

**Table 5** $\psi$ erosion coefficients and $\alpha$ imperfection factors for simple imperfections

| Imperfection | RSN125×3.2 | | Imperfection | RSN125×3.2 | |
|---|---|---|---|---|---|
| | $\psi$ | $\alpha$ | | $\psi$ | $\alpha$ |
| ds – 0.5 $t$ | 0.236 | 0.078 | EZ -6 | 0.313 | 0.152 |
| ds – 1.0 $t$ | 0.339 | 0.185 | EZ -4 | 0.272 | 0.108 |
| ds – 1.5 $t$ | 0.398 | 0.280 | EZ -2 | 0.210 | 0.059 |
| da – 0.5 $t$ | 0.152 | 0.029 | EZ +2 | 0.216 | 0.063 |
| da – 1.0 $t$ | 0.245 | 0.085 | EZ +4 | 0.255 | 0.093 |
| da – 1.5 $t$ | 0.321 | 0.162 | EZ +6 | 0.285 | 0.121 |
| f – $L/750$ | 0.240 | 0.081 | EY-EZ 0 | 0.157 | 0.031 |
| f – $L/1000$ | 0.216 | 0.063 | EY-EZ +6 | 0.321 | 0.162 |
| f – $L/1500$ | 0.181 | 0.043 | EY-EZ +4 | 0.276 | 0.112 |
| ft | 0.240 | 0.081 | EY-EZ +2 | 0.215 | 0.063 |
| EY +2 | 0.169 | 0.037 | EY-EZ -2 | 0.223 | 0.068 |
| EY +4 | 0.196 | 0.051 | EY-EZ -4 | 0.270 | 0.106 |
| EY +6 | 0.224 | 0.069 | EY-EZ -6 | 0.307 | 0.145 |

**Table 6** $\psi$ erosion coefficients and $\alpha$ imperfection factors for coupled imperfections

| Imperfection | $\psi$ | $\alpha$ | $\psi$ | $\alpha$ | $\psi$ | $\alpha$ | $\psi$ | $\alpha$ |
|---|---|---|---|---|---|---|---|---|
| | f – $L/750$, ds – $0.5t$ | | f – $L/750$, ds – $1.5t$ | | f – $L/1500$, ds – $0.5t$ | | f – $L/1500$, ds – $1.5t$ | |
| EY 2 | 0.339 | 0.185 | 0.440 | 0.368 | 0.302 | 0.139 | 0.422 | 0.328 |
| EY 4 | 0.342 | 0.189 | 0.442 | 0.373 | 0.305 | 0.142 | 0.423 | 0.330 |
| EY 6 | 0.346 | 0.195 | 0.443 | 0.375 | 0.310 | 0.148 | 0.425 | 0.334 |
| EZ 6 | 0.425 | 0.334 | 0.493 | 0.510 | 0.411 | 0.305 | 0.483 | 0.480 |
| EZ 4 | 0.404 | 0.292 | 0.479 | 0.469 | 0.384 | 0.255 | 0.467 | 0.436 |
| EZ 2 | 0.376 | 0.241 | 0.461 | 0.420 | 0.350 | 0.201 | 0.447 | 0.385 |
| EZ -2 | 0.279 | 0.115 | 0.413 | 0.309 | 0.174 | 0.039 | 0.387 | 0.260 |
| EZ -4 | 0.194 | 0.050 | 0.374 | 0.238 | 0.228 | 0.072 | 0.326 | 0.168 |
| EZ -6 | 0.240 | 0.081 | 0.276 | 0.112 | 0.264 | 0.101 | 0.261 | 0.098 |
| EY-EZ 0 | 0.240 | 0.081 | 0.440 | 0.368 | 0.301 | 0.138 | 0.421 | 0.326 |
| EY-EZ 6 | 0.430 | 0.345 | 0.495 | 0.517 | 0.414 | 0.311 | 0.485 | 0.486 |
| EY-EZ 4 | 0.406 | 0.295 | 0.480 | 0.472 | 0.386 | 0.258 | 0.467 | 0.436 |
| EY-EZ 2 | 0.377 | 0.243 | 0.462 | 0.422 | 0.351 | 0.202 | 0.447 | 0.385 |
| EY-EZ -2 | 0.280 | 0.116 | 0.413 | 0.309 | 0.182 | 0.043 | 0.387 | 0.260 |
| EY-EZ -4 | 0.218 | 0.065 | 0.376 | 0.241 | 0.247 | 0.086 | 0.330 | 0.173 |
| EY-EZ -6 | 0.271 | 0.107 | 0.298 | 0.135 | 0.289 | 0.125 | 0.285 | 0.121 |

As observed in Tab. 4, for RS95×2.6 section there is no classical buckling mode interaction. Further, the present imperfection study will be focused on RSN125×3.2 only. Tab. 5 presents the considered simple imperfections, sectional, global and loading eccentricities for RSN125×3.2 section together with $\psi$ erosion coefficient and $\alpha$ imperfection factors for simple imperfections.

In Tab. 5 can be easily observed that, for simple imperfections, symmetric distortion imperfection and major axis eccentricities give higher values for erosion coefficient than those corresponding to flexural and flexural–torsional imperfections.

Tab. 6 presents the coupled imperfections considered for the RSN125×3.2 section, i.e. f – $L/750$, ds – $0.5t$; f – $L/750$, ds – $1.5t$; f – $L/1500$, ds – $0.5t$ and f – $L/1500$, ds – $1.5t$, combinations coupled with various types of eccentricities. It is easy to observe that the combination (f – $L/750$, ds – $1.5t$) of imperfections is the most critical one. However, statistically is not recommended to combine all imperfections to cumulate their negative effects, because their random compensation.

A precise framing for coupled instabilities is very important in order to choose a suitable design strategy. For weak and moderate interaction class, simple design methods based on safety coefficients can be used. In case of strong and very strong interaction, special design methods must be developed [20].

It can be observed that for the case of RSN125×3.2 pallet rack section, the computed erosion can classify the section into medium up to very strong interaction, depending on the considered imperfection.

## 5. Conclusions

Both experimental tests and numerical simulations have proven the negative influence of both interaction between distortional and overall buckling and geometrical imperfections on the ultimate capacity of perforated pallet rack sections in compression in the interactive range, especially for the case of sections analysed in this paper.

The ECBL approach is an excellent method that allows for the evaluation of $\psi$ erosion coefficients and $\alpha$ imperfection factors, as result of interactive buckling. It applies for the interaction of sectional (local or distortional buckling) with global (flexural or flexural–torsional) instability modes, using a limited number of experimental tests.

In order to reduce the number of experimental tests, a rational sensitivity analysis done using calibrated and validated numerical models can be used in order to determine the most detrimental imperfections to be considered for the numerical modelling. Moreover, using correctly calibrated numerical models, ECBL is a perfect method to perform a sensitivity analysis and to obtain the maximum erosion coefficient and corresponding imperfection factor for a given section, with or without perforations.

Performing a sensitivity analysis for RSN125×3.2 cross-section, it is easy to observe that for uncoupled imperfections, symmetric distortion imperfection and major axis eccentricities give higher values for erosion coefficient than those corresponding to flexural and flexural-torsional imperfections. For the case of coupled imperfections, it is easy to observe that (f – $L/750$, ds – $1.5t$) combination of imperfections is the most critical one. However, statistically is not recommended to combine all imperfections to cumulate their negative effects, because their random compensation.

In conclusion, related to the imperfection scenarios to be adopted in numerical simulations, it is compulsory to be estimated by means of reliability analysis, in order to get results for a given failure probability. On this purpose, future research

should be done in order to find values for reliability index that could be associated with the erosion classes of mode interaction.

## References


[1] **Rondal, J.**: Thin–walled structures – General Report, *Stability of steel structures*, Budapest, Hungary: Akademiai Kiado, pp. 849–66, **1988**.

[2] **Schafer, B. W. and Peköz, T.**: Computational modelling of cold–formed steel characterising geometric imperfections and residual stresses, *J. Constructional Steel Research*, 47(3), pp. 193–210, **1998**.

[3] **Abdel–Rahman, N. and Sivakumaran, K. S.**: Material properties models for analysis of cold–formed steel members, *J. Struct. Eng.*, ASCE, 123(9), pp. 1135–1143, **1997**.

[4] **Moen, C. D., Igusa, T. and Schafer, B. W.**: Prediction of residual stresses and strains in cold–formed steel members, *Thin–Walled Structures*, 46, pp. 1274–1289, **2008**.

[5] **Dubina, D., Ungureanu, V. and Rondal, J.**: Numerical modelling and codification of imperfections for cold–formed steel members analysis, *Steel and Composite Structures*, Vol. 5, No. 6, pp. 515–533, **2005**.

[6] **Dubina, D and Ungureanu, V.**: Effect of imperfections on numerical simulation on instability behaviour of cold–formed steel members, *Thin–Walled Structures*, 40(3), pp. 239–262, **2002**.

[7] **Rasmussen, K. J. R. and Hancock, G. J.**: Geometric imperfections in plated structures subject to interaction between buckling modes, *Thin–Walled Structures*, 6, pp. 433–452, **1988**.

[8] **Schafer, B. W., Grigoriu, M. and Peköz, T.**: A probabilistic examination of the ultimate strength of cold-formed steel elements, *Thin–Walled Structures*, 31(4), pp. 271–288, **1998**.

[9] **Rasmussen, K. J. R.**: Numerical simulations and computational models in coupled instabilities, Proc. of the $2^{nd}$ *Int. Conf. on Coupled Instabilities in Metal Structures*, CIMS'96, pp. 45–60, **1996**.

[10] **Sridharan, S.**: Numerical simulation and computational models for coupled instabilities, Proc. of the $3^{rd}$ *Int. Conf. on Coupled Instabilities in Metal Structures*, CIMS'2000, pp. 61–72, **2000**.

[11] **Schafer, B. W.**: Computational modelling of cold–formed steel, Proc. of the $5^{th}$ *Int. Conf. on Coupled Instabilities in Metal Structures*, CIMS'2008, pp. 53–60, **2008**.

[12] **Adany, S. and Schafer, B. W.**: A full modal decomposition of thin–walled, single–branched open cross–section members via constrained finite strip method, *J. Constructional Steel Research*, 64(1), pp. 12–29, **2008**.

[13] **Bebiano, R., Pina, P., Silvestre, N. and Camotim D.**: GBTUL – Buckling and vibration analysis of thin–walled members, DECivil/IST, Technical University of Lisbon, http://www.civil.ist.utl.pt/gbt, **2008**.

[14] **Camotim, D., Basaglia, C. and Silvestre, N.**: GBT buckling analysis of thin–walled steel frames: A state of the art report, *Thin–Walled Structures*, 48(10-11), pp. 726–743, **2010**.

[15] **Camotim, D. and Dinis, P. B.**: Coupled instabilities with distortional buckling in cold–formed steel lipped channel columns, *Thin–Walled Structures*, 48(10–11), pp. 771–785, **2010**.

[16] **Loughlan, J., Yidris, N. and Jones, K.**: The failure of thin–walled lipped channel compression members due to coupled local–distortional interactions and material yielding, *Thin–Walled Structures*, vol. 61, pp. 14–21, **2012**.

[17] **Armani, P., Baldassino, N. and Zandonini, R.**: Study of the response of uprights of pallet racks under compression. Proc. of the $6^{th}$ *Int. Conf. on Thin Walled Structures*, Timisoara, Romania, Vol. 2, pp. 772–778, **2011**.

[18] **Casafont, M., Caparrós, F., Pastor, M., Roure, F. and Bonada, J.**: Linear buckling analysis of perforated steel storage rack columns with the finite strip method, Proc. of the $6^{th}$ *Int. Conf. on Thin Walled Structures*, Timisoara, Romania, Vol. 2, pp. 787–794, **2011**.

[19] **Bonada, J., Casafont, M., Roure, F. and Pastor, M. M.**: Selection of the initial geometrical imperfection in nonlinear FE analysis of cold–formed steel rack columns, *Thin–Walled Structures*, 51, pp. 99–111, **2012**.

[20] **Dubina, D.**: The ECBL approach for interactive buckling of thin–walled steel members, *Steel & Composite Structures*, 1(1), pp. 75–96, **2011**.

[21] **Crisan, A.**: Buckling strength of cold formed steel sections applied in pallet rack Structures, *PhD thesis*, "POLITEHNICA" University of Timisoara, Civil Engineering Faculty, Ed. Politehnica, Seria 5: Inginerie Civila, no. 76, **2011**.

[22] **Crisan, A., Ungureanu, V. and Dubina, D.**: Behaviour of cold–formed steel perforated sections in compression. Part 1 – Experimental investigations, *Thin–Walled Structures*, Vol. 61, pp. 86–96, **2012**.

[23] **Crisan, A., Ungureanu, V. and Dubina, D.**: Behaviour of cold–formed steel perforated sections in compression. Part 2 – Numerical investigations and design consideration, *Thin–Walled Structures*, Vol. 61, pp. 97–105, **2012**.

[24] **EN15512:2009: Steel static storage systems – Adjustable pallet racking systems – Principles for structural design**, *CEN*, Brussels, **2009**.

[25] **European Recommendation for the Design of Light Gauge Steel Members**, *ECCS*, Brussels, **1978**.

[26] **EN1090-2:2008. Execution of steel structures and aluminium structures – Part 2: Technical requirements for steel structures**, *CEN*, Brussels, **2009**.

[27] **AS4100-1990: Australian Standard: Steel Structures**, Homebush, Australia, **1990**.